J Mater Sci (2018) 53:12961–12973

Electronic materials

Role of vacancy defects on the lattice thermal conductivity in In_2O_3 thermoelectric nanocrystals: a positron annihilation study

H. F. He[1], B. Zhao[1], N. Qi[1], B. Wang[1], Z. Q. Chen[1,*], X. L. Su[2], and X. F. Tang[2]

[1] *Hubei Nuclear Solid Physics Key Laboratory, Department of Physics, Wuhan University, Wuhan 430072, China*
[2] *State Key Laboratory of Advanced Technology for Materials Synthesis and Processing, Wuhan University of Technology, Wuhan 430070, China*

Received: 16 April 2018
Accepted: 4 June 2018
Published online: 11 June 2018

ABSTRACT

High purity In_2O_3 nanopowders were subjected to different thermal treatments to investigate the role of defects on the lattice thermal conductivity. The powders were first treated by spark plasma sintering (SPS) at 700 °C and annealed in air between 700 and 1300 °C. X-ray diffraction measurements show that the samples are single phase, and the diffraction peaks become sharper with increasing of annealing temperature, indicating improvement in crystallinity and increase in grain size. The In_2O_3 nanopowders were also treated by SPS sintering at different temperatures without subsequent annealing. On the contrary, the average grain size of In_2O_3 treated by SPS has no obvious change with the increase in sintering temperatures. Positron annihilation measurements reveal large amounts of monovacancies and vacancy clusters in the In_2O_3 nanocrystals. The monovacancies gradually recover and the vacancy clusters transform into smaller vacancies with increasing annealing or sintering temperatures. The lattice thermal conductivity increases with the increase in annealing or sintering temperature, which shows close correlation with the recovery of vacancy defects after heat treatment. This gives us strong evidence that vacancy defects play an important role on the suppression of lattice thermal conductivity in nanostructured thermoelectric materials.

Introduction

Based on the principles of Seebeck effect, Peltier effect and Thomson effect, thermoelectric (TE) materials can convert temperature difference into electric voltage and vice versa. They have found potential application in waste heat recovery and solid-state cooling [1–3]. The utilization of waste heat energy by this technique has potential contribution to the relief of the dependence on fossil fuels and the improvement in environmental pollution. The performance of TE materials is evaluated by the dimensionless

Address correspondence to E-mail: chenzq@whu.edu.cn

https://doi.org/10.1007/s10853-018-2544-5

figure of merit $ZT = \sigma S^2 T/\kappa$, where S, T, σ and κ are Seebeck coefficient, absolute temperature, electric conductivity and thermal conductivity, respectively.

It is clear that high ZT thermoelectric materials should possess simultaneously large Seebeck coefficient, high electric conductivity and low thermal conductivity. However, these three parameters are not independently controllable, and they are determined by the detailed characteristics of a system, such as carrier concentration, crystalline structure and energy band. [4, 5]. So far, the effective way to increase the dimensionless figure of merit is the reduction in thermal conductivity rather than the improvement in power factor (σS^2). The total thermal conductivity κ is the sum of lattice thermal conductivity κ_L and electronic thermal conductivity κ_E as: $\kappa = \kappa_L + \kappa_E$, within which the electronic thermal conductivity is related to the electric conductivity by the Wiedemann–Franz law ($\kappa_E = L\sigma T$, where L is the Lorentz constant).

One effective way to decrease the thermal conductivity is to minimize the lattice thermal conductivity κ_L, which is the only independently controllable parameter. This can be accomplished by several approaches, such as the alloy scattering by substituting host atoms with guest dopants, or the "rattle" scattering in skutterudites and clathrates [6]. In case of alloy scattering, it can efficiently increase ZT by enhancing the phonon scattering. The scattering factor A of the guest atom is related to the mass difference of the host and guest atoms as follows [7–9]:

$$A = \frac{\Omega_0}{4\pi v^2} x(1-x)\left(\frac{\Delta M}{M}\right)^2, \quad (1)$$

where Ω_0 is the volume of the unit cell, v is the lattice sound velocity, x is the fraction of the guest atom, ΔM is the atomic mass difference between the guest and host atoms, and M is the average mass of the cell. It can be seen that the mass difference ΔM plays a key role on the reduction in the lattice thermal conductivity, and the larger the mass difference, the larger will be the reduction in κ_L. The maximal mass difference can be achieved by introducing vacancies on one or more lattice sites; therefore, the maximal phonon scattering by mass fluctuation can be achieved. Up to now there are several reports which suggest possible effects of vacancy defects on the thermoelectric properties in various materials [10–16].

It was found that nanostructured thermoelectric materials can also efficiently reduce the lattice thermal conductivity [17–20]. This is supposed to be due to the phonon scattering at nanoscaled interfaces, which is especially effective for the mid- to long-wavelength phonons, since the grain size is smaller than the phonon mean free path. On the other hand, due to the high fraction of interface region in the nanostructured materials, there are large amounts of defects in these regions, which may also act as phonon scattering centers. However, up to now it is still difficult to confirm the contribution of these interfacial defects to the reduction in lattice thermal conductivity in nanostructured materials, since there is a lack of appropriate probe which is particularly sensitive to the defects in the interface region.

Oxide-based semiconductors are regarded as promising thermoelectric materials because of their superb structural and chemical stability [21]. They can operate at high temperatures in oxygen-containing atmosphere. Among the oxides, indium oxide (In_2O_3) is a wide band gap semiconductor, which is one candidate for the thermoelectric materials [22]. By co-doping with Zn and Ce, a ZT value of 0.4 at 1050 K has been achieved in In_2O_3 with grain size of 50 nm [23]. A higher ZT value of 0.7 can be obtained when the grain size is further decreased to 20 nm [23]. This suggests that either grain boundary or defect scattering are responsible for the increase in ZT value in naostructured In_2O_3. The role of defects may play a more important role on the reduction in lattice thermal conductivity, since the phonon mean free path will decrease significantly when the oxides work at temperatures higher than 1000 K, and the contribution of grain boundary scattering decreases drastically.

In order to verify the role of vacancies on the lattice thermal conductivity, a proper method to characterize the atomic-scaled defect is necessary. Positron annihilation spectroscopy (PAS) has been proved to be a very sensitive probe to investigate vacancy defects in materials [24, 25]. Positrons are trapped preferentially by vacancy defects where electron density is lower than the perfect bulk crystal. Positron annihilation parameters at vacancy defects are different from those in the bulk state. Therefore, identification of vacancies is very straightforward. A longer positron lifetime or narrower Doppler

broadening of the annihilation radiation than the defect-free bulk state thus indicates existence of vacancy defects. Positrons are particularly sensitive to the interfacial defects in nanocrystals. This is because that the grain size is usually smaller than the positron diffusion length (typically about 100 nm). The defect-rich grain boundaries are effective positron trapping centers, so almost all the positrons will diffuse to these regions and annihilate there. In this sense, positron is a self-seeking probe for the interfacial defects, which greatly enhances the sensitivity of positron to interfacial defects. Several works have been published about PAS studies in various nanomaterials [26–33].

In this paper, we studied the effect of thermal treatment on the interfacial defects in In_2O_3 nanocrystals. Positron lifetime, X-ray diffraction (XRD) and scanning electron microscope (SEM) were measured for a comprehensive understanding of the structure and defect characteristics of In_2O_3 nanocrystals after thermal treatment. The electrical properties and thermal conductivity were also studied. An intimate correlation between the phonon thermal conductivity and vacancy defects has been observed.

Experiment

Pure In_2O_3 nanopowders were purchased from Beijing DK nanotechnology Co. LTD with purity $\geq 99.9\%$ and grain size of about 20 nm. The powders were hand milled in an agate mortar with pestle for about 2 h, then part of the powders were treated by a spark plasma sintering (SPS) process at 700 °C for 5 min under pressure of 80 Mpa. After sintering, the samples were further annealed in vacuum in a furnace at 700, 900, 1000, 1100, 1200 and 1300 °C for 2 h, respectively. The other part of powders were treated by a SPS process at six temperatures of 500, 600, 700, 800, 900 and 1000 °C for 5 min under pressure of 80 Mpa.

Positron lifetime measurements were performed using a conventional fast–fast coincidence system with a time resolution of 220 ps in full width at half maximum. $A^{22}Na$ positron source with activity of about 20 μCi was deposited on a Kapton foil with thickness of about 7.5 μm and was then covered by another identical Kapton foil. The source was sandwiched between two identical samples pellets for measurements. Two lifetime spectra with total counts of 10^6 for each were measured for every sample after different treatment to ensure the reliability of the measurements. X-ray diffraction (PANalytical Xpert Pro) measurements were conducted using Cu Kα radiation ($\lambda = 0.15418$ nm). Scanning electron microscopy (FEI SIRION) was used to investigate the morphology of the specimens after sintering and annealing at different temperatures. Electrical resistivity ρ and Seebeck coefficient S were measured by a standard four-probe method (ZEM-3, Ulvac Riko, Inc.) under a low-pressure inert gas (He) atmosphere. The thermal conductivity κ was calculated from the measured thermal diffusivity (D), specific heat (C_p), and density (d) by the formula $\kappa = DC_pd$. The thermal diffusivity D was measured by the laser flash diffusivity method using a Netzsch LFA-457 system. The relative bulk density d was measured by the Archimedes method, and the specific heat C_p was measured by a power compensation differential scanning calorimeter (DSC Q20, TA Instruments, USA) in an Ar atmosphere.

Results and discussion

Effect of thermal annealing treatment

Figure 1 shows the XRD patterns measured for the In_2O_3 nanocrystals after SPS treatment at 700 °C and annealed at different temperatures. The samples all show cubic bixbyite-type structure of In_2O_3 (JCPDS Card No. 06-0416) without impurity phase within the detection limit of XRD. The peaks grow higher and become narrower with increasing annealing temperature. This implies that the crystallinity of the sample becomes better after annealing. The average grain size of the annealed In_2O_3 samples is estimated by Scherrer's formula [34]:

$$D_{hkl} = K\lambda/\beta\cos\theta, \quad (2)$$

where D_{hkl} is the grain size perpendicular to the (hkl) plane, K is the shape factor (usually taken as 0.9), λ is the X-ray wavelength, β is the linewidth at half maximum intensity of the XRD peak (every observed peak in the spectra was fitted with a Gaussian function), and θ is taken as the Bragg angle [34]. The contribution of instrumental broadening in β has been taken into consideration using the standard method. The average grain size of In_2O_3 as a function

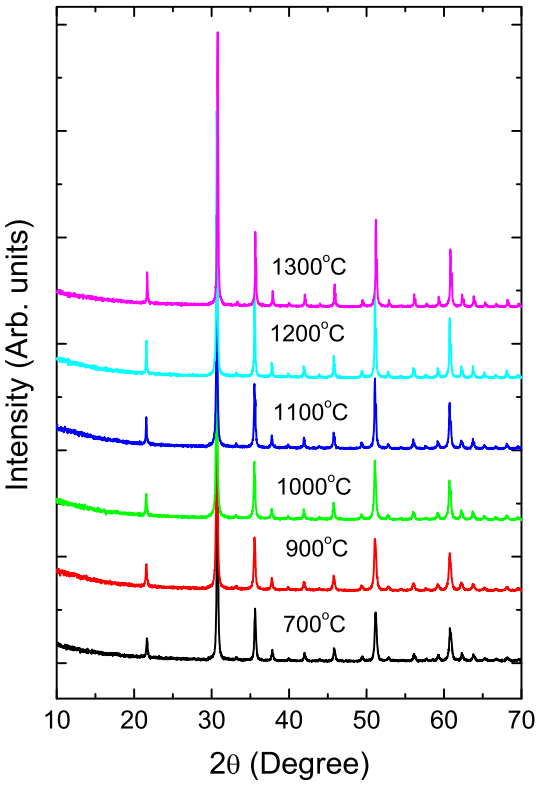

Figure 1 2θ scan of XRD patterns for SPS sintered In_2O_3 nanocrystals after annealing at different temperatures.

of annealing temperature is shown in Fig. 2. There is no obvious grain growth after annealing the SPS-treated sample up to 1000 °C with an average grain size of about 35 nm. With increasing annealing temperatures above 1000 °C, the grain size shows continuous increase and reaches about 72 nm after annealing at 1300 °C.

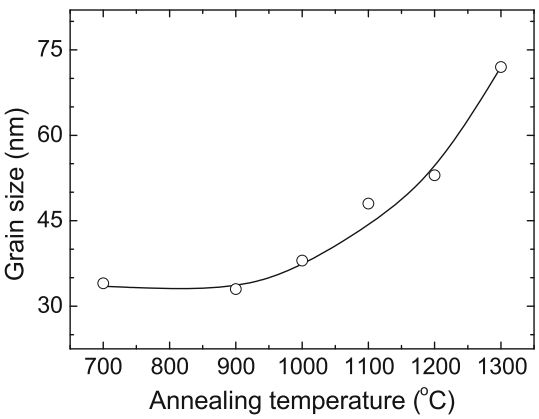

Figure 2 Variation of the grain size of SPS sintered In_2O_3 nanocrystals after annealing at different temperatures.

The morphology of fractured cross section of the samples annealed at some selected temperatures (700, 900, 1100 and 1300 °C) was examined by the scanning electron microscope. The corresponding SEM images are shown in Fig. 3a–d. The average particle size of the In_2O_3 samples annealed at 700 and 900 °C is about 80 nm, which is about two times of the grain size calculated from XRD patterns. This indicates that most particles are small clusters of In_2O_3 crystalline grains. After annealing at 1100 °C, the particle morphologies become inhomogeneous. The smallest particle has a diameter of about 50 nm which is consistent with the grain size estimated from the XRD pattern, while the largest one has a diameter of about 500 nm. The larger particles seem to be clusters composed of dozens of small grains. After annealing at 1300 °C, significant reorganization of crystallites can be observed, as shown in Fig. 3d. The particle size ranges from 1 to 3 μm which is much larger than the estimated grain size, indicating further agglomeration of grains after annealing at 1300 °C.

A detailed study of the microstructural defects in the In_2O_3 nanocrystals was performed by positron lifetime measurements. All the measured positron lifetime spectra were resolved into two components by the computer program PATFIT [35], and the contribution of the background and source component (positron annihilation lifetime and intensity in Kapton foils) was subtracted. Figure 4 shows positron lifetime τ_1, τ_2, intensity I_2 and the average lifetime τ_{av} of τ_1 and τ_2 as a function of annealing temperature. The average positron lifetime τ_{av} is calculated by the following formula:

$$\tau_{av} = \tau_1 I_1 + \tau_2 I_2. \quad (3)$$

The shorter positron lifetime τ_1 is generally attributed to the free annihilation of positrons without trapping by defects [36, 37]. However, in some disordered systems, annihilation of positrons in smaller vacancies such as monovacancies may also contribute to τ_1. The reported positron lifetime in perfect In_2O_3 lattice (bulk lifetime τ_b) is about 183 ps [38]. In our result, τ_1 is obviously longer than the bulk lifetime τ_b. This suggests that τ_1 is a weighted average lifetime of free and trapped positrons. As shown in Fig. 4, the longer lifetime component τ_2 also decreases monotonically from about 435 to 277 ps with increasing annealing temperature. The ratio of τ_2/τ_b has the highest value of 2.37 for the sample annealed at 700 °C. This

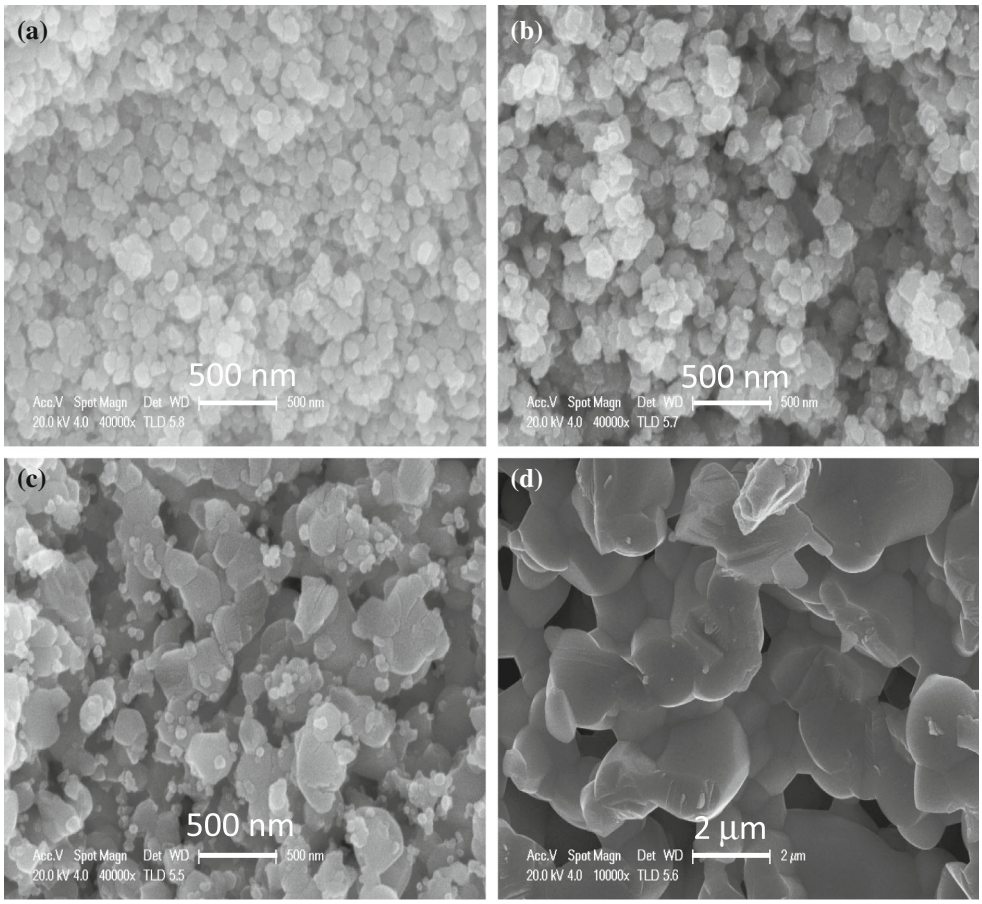

Figure 3 SEM image of SPS sintered In_2O_3 nanocrystals after annealing at **a** 700 °C; **b** 900 °C; **c** 1100 °C; **d** 1300 °C.

suggests that τ_2 is due to positron trapping at some larger vacancies, such as vacancy clusters, since it is much longer than the bulk lifetime of 183 ps.

According to the two-state positron trapping model [39], the measured lifetime τ_1 should be related to the trapping rate κ by the following equation:

$$\tau_1 = \frac{1}{\lambda_b + \kappa}, \tag{4}$$

where λ_b is the inverse of positron bulk lifetime τ_b, and the positron trapping rate κ is proportional to the defect concentration C_d ($\kappa = \mu C_d$, where μ is the trapping coefficient). It can be seen from Fig. 4 that the lifetime τ_2 shows continuous decrease with increasing annealing temperature, and the average lifetime also shows similar decrease. This suggests that the positron trapping rate most probably decreases after annealing. According to Eq. (3), if we suppose that positrons are trapped by only one type of defects (two-state trapping model), i.e., the lifetime τ_1 is purely the free annihilation lifetime of positrons, then it should be shorter than τ_b, and it will increase with annealing temperature due to the decrease in positron trapping rate κ. However, in the present paper, τ_1 is longer than τ_b, and it shows decrease from about 234 ps to about 196 ps with increasing annealing temperature from 700 to 1300 °C as shown in Fig. 4. The opposite trend of τ_1 confirms that it is a mixture of free annihilation lifetime and trapped lifetime at small vacancies. The decrease in τ_1 is just due to the recovery of these small vacancies such as In monovacancies.

In order to estimate the size of vacancy defects corresponding to τ_2, we calculated positron lifetime of vacancy clusters with various size in In_2O_3 using the atomic superposition method [40]. The vacancy clusters contain different number of In–O vacancy pairs, since they contain less dangling bonds and then are more stable in In_2O_3 structures. The calculated positron lifetimes for different vacancy clusters are shown in Fig. 5. The results of In monovacancy are also presented. The positron bulk lifetime in In_2O_3 is about 161 ps, which is shorter than the experimental value. With increasing size of vacancy clusters, positron lifetime shows continuous increase.

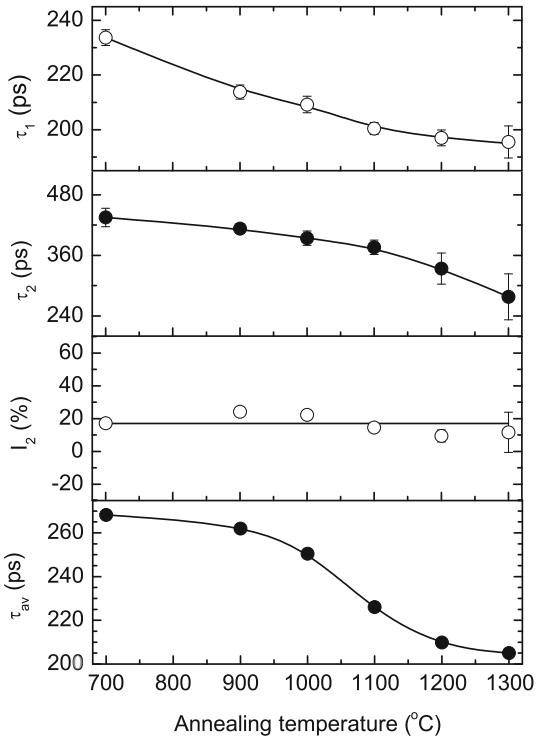

Figure 4 Positron lifetime τ_1, τ_2, intensity I_2 and the average lifetime τ_{av} in SPS sintered In_2O_3 nanocrystals as a function of annealing temperature.

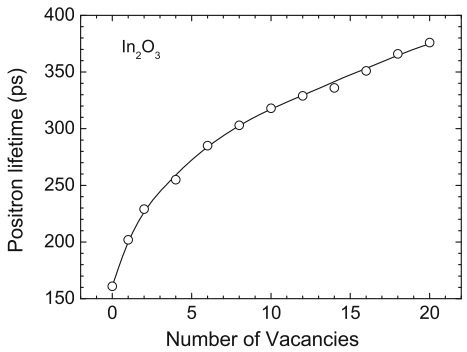

Figure 5 Calculated positron lifetimes in vacancies with different size in In_2O_3.

The ratio of defect lifetime to the bulk lifetime (τ_2/τ_b) is a relatively reliable parameter to evaluate the size of vacancy defects. For the sample annealed at 700 °C, the experimental value of τ_2/τ_b is 2.37, which corresponds to a vacancy cluster with about ten pairs of atoms of In and O. After annealing at 1300 °C, τ_2 decreases to about 277 ps, and according to the theoretical calculation, the corresponding size of defect reduces to small vacancy cluster which contains only one or two pairs of In and O, indicating that larger vacancy clusters gradually transform into smaller vacancy clusters with increasing annealing temperature. The transformation of clusters suggests that the larger vacancy clusters becomes unstable at higher temperature. As shown in Fig. 4, the average positron lifetime τ_{av} decreases monotonically from about 270 to 205 ps by almost 65 ps after annealing at 1300 °C. This is a more reliable parameter to evaluate any change of the defect properties, because it is insensitive to the decomposition of positron lifetime spectrum by the computer program PATFIT. Thus, it further confirms the recovery of larger vacancy clusters after annealing.

The decrease in positron lifetime shown in Fig. 4 might be also due to the increase in grain size after annealing, since increase in grain size will cause decrease in the fraction of interface region, therefore, the fraction of positron trapping and annihilating at interfacial defects will also decrease. For our samples annealed at different temperatures, the grain size did show some increase from about 35 nm to about 72 nm. But even for grain size of 72 nm, the radius of the grain (36 nm) is still shorter than the positron diffusion length (typically $\sim$100 nm). Then almost all the positrons will still diffuse to the interface region and annihilate there. So if the defects themselves do not show any recovery, the increase in grain size to only 72 nm will not cause sufficient decrease in positron lifetime. So we believe that the decrease in positron lifetime is due to recovery of interfacial defects, and is less likely due to the increase in grain size.

Figure 6 shows the temperature dependence of electrical resistivity ρ, Seebeck coefficient S, total lattice thermal conductivity κ and lattice thermal conductivity κ_L of In_2O_3 nanocrystals after annealing at different temperatures. For all annealed samples, the Seebeck coefficients are negative, and they decrease almost linearly with increasing measurement temperatures, but they are not very sensitive to the annealing temperatures. The negative Seebeck coefficient indicates that the dominant charge carrier of In_2O_3 samples is electron. This is in agreement with the n-type conductivity of undoped In_2O_3, though the origin of the native donor is still unclear [41]. All the samples show an increasing trend in electrical resistivity with increasing measuring temperature, indicating a metallic conducting behavior. On the other hand, the electrical resistivity decreases monotonically with increasing annealing temperature, which indicates that the electrical resistivity is

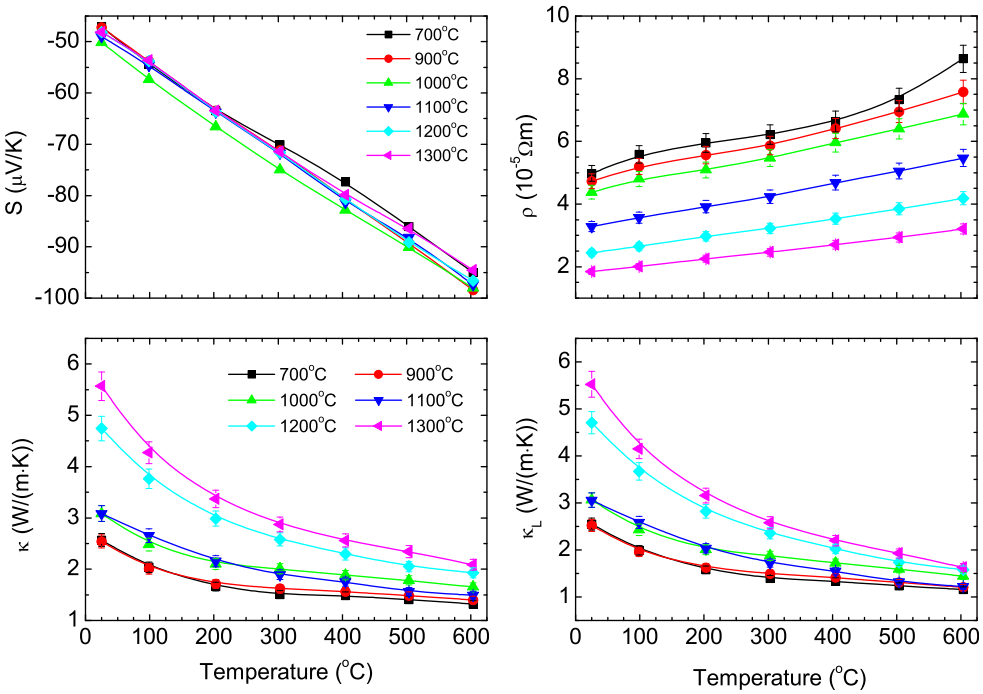

Figure 6 Seebeck coefficient S, electrical resistivity ρ, total thermal conductivity κ and lattice thermal conductivity κ_L of SPS sintered In_2O_3 nanocrystals after annealing at different temperatures between 700−1300 °C.

quite sensitive to the annealing temperature. This is a common phenomenon in oxides, in which the electrical conductivity will increase abruptly after high-temperature annealing due to the production of donor-type defects such as In interstitials or oxygen vacancies. The increase in the carrier mobility might be another reason for the decrease in the resistivity after annealing, since the crystallinity shows improvement as indicated by XRD measurements.

For all the annealed samples, the thermal conductivity shows an overall decrease with increasing measurement temperature. Furthermore, in the whole measurement temperature range of 25−600 °C, κ shows an increasing trend with increasing annealing temperature. At about 25 °C, the value of κ increases from 2.6 to 5.6 $Wm^{-1}K^{-1}$ after annealing at 1300 °C, and at 600 °C it increases from 1.3 to 2.1 $Wm^{-1}K^{-1}$. The total thermal conductivity κ contains contribution from the lattice thermal conductivity κ_L and electronic thermal conductivity κ_E by the formula $\kappa = \kappa_L + \kappa_E$. The electronic thermal conductivity can be calculated from the measured electric conductivity by using the Wiedemann–Franz law ($\kappa_E = L\sigma T$), where the Lorenz number $L = 2.45 \times 10^{-8}$ $W\Omega K^{-2}$. The lattice thermal conductivity is then estimated after subtracting the calculated electronic thermal conductivity from the total thermal conductivity and is also plotted in Fig. 6. It is clear that the change of lattice thermal conductivity with annealing temperature is nearly the same as the total thermal conductivity, indicating that the contribution of electronic thermal conductivity is very small. Comparing with the positron annihilation measurements, we can find that the increase in lattice thermal conductivity is closely correlated with the recovery process of vacancy defects after annealing. This implies that the phonon scattering by the vacancy-type defects is an effective approach to reduce the lattice thermal conductivity of In_2O_3 nanocrystals.

Figure 7 shows ZT value of the In_2O_3 nanocrystals as a function of measurement temperature after

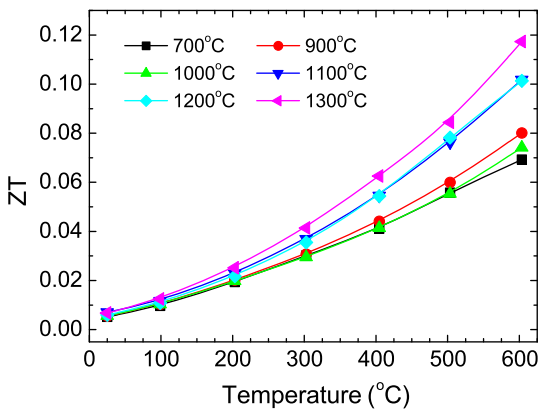

Figure 7 ZT factor of SPS sintered In_2O_3 nanocrystals after annealing at different temperatures between 700−1300 °C.

annealing at different temperatures. It is clear that the ZT value shows overall increase with increasing annealing temperature in the whole measurement temperature range of 25−600 °C. At 600 °C, it increases from about 0.07 to about 0.12 after annealing at 1300 °C. This is primarily due to the increase in the electrical conductivity after annealing. Though the thermal conductivity shows substantial increase due to the recovery of vacancies after annealing, the electrical conductivity shows a larger increase, thus leads to an increase in ZT value after annealing the sample.

Effect of SPS sintering treatment

Figure 8 shows the XRD patterns of In_2O_3 nanocrystals after SPS treatment at different temperatures. All the samples show single phase which can be indexed by the cubic bixbyite-type structure of In_2O_3 (JCPDS Card No. 06-0416), and the peaks have no obvious change after sintering. The average grain size is calculated by Eq. (1) and its variation with SPS temperature is shown in Fig. 9. Sintering at different temperatures has no apparent effect on the growth of grain size. After sintering at 500 °C, the average grain size is estimated to be around 33 nm, and it has only a slight increase by about 12 nm when the sintering temperature increases to 900 °C.

SEM images of fractured cross section of the In_2O_3 compounds sintered at temperatures of 500, 700, and 1000 °C are shown in Fig. 10. The average particle size of the sample sintered at 700 °C is about 60 nm, and it increases with increasing sintering temperature. When the sintering temperature reaches 1000 °C, the average particle size is about 400 nm, which indicates significant agglomeration of small crystalline grains, while the grain size keeps almost unchanged as revealed by XRD measurements.

Figure 11 shows the positron lifetime τ_1, τ_2, the intensity I_2 as well as the average lifetime τ_{av} as a function of the sintering temperature. It is seen that τ_1 keeps almost constant at about 200 ps before the sintering temperature reaches 800 °C, then it begins to decrease, which indicates recovery of some small defects such as monovacancies. The lifetime τ_2 also keeps unchanged with sintering temperature below 700 °C. In this temperature range, the value of τ_2/τ_b is about 2.09. By comparing with the result of theoretical calculation, the corresponding defect is estimated to be vacancy clusters containing 7 pairs of In and O. When the sintering temperature is above 700 °C, τ_2 shows continuous decrease, and the ratio τ_2/τ_b decreases to about 1.43 when sintering temperature reaches 1000 °C. This ratio corresponds to divacancy which contains one pair of In and O. During the whole sintering temperature range, the intensity I_2 has no obvious change. The average positron lifetime shows only slight decrease when the sintering

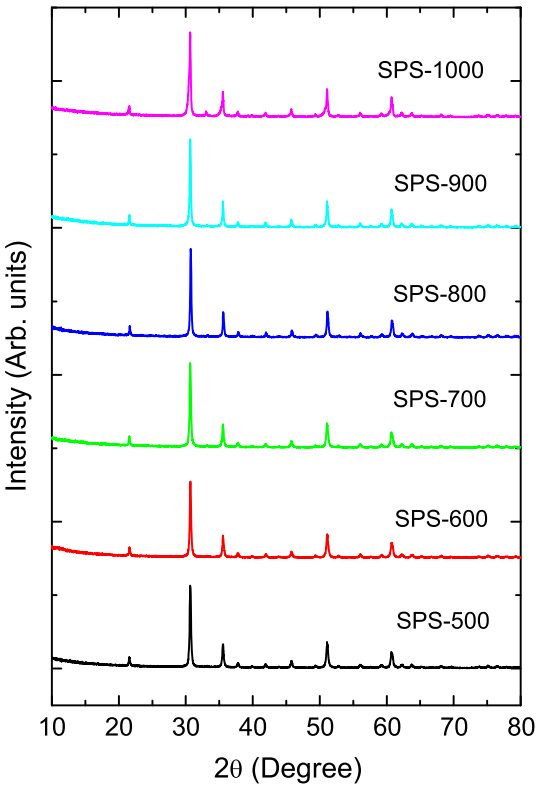

Figure 8 2θ scan of XRD patterns for In_2O_3 nanocrystals after SPS treatment at different temperatures.

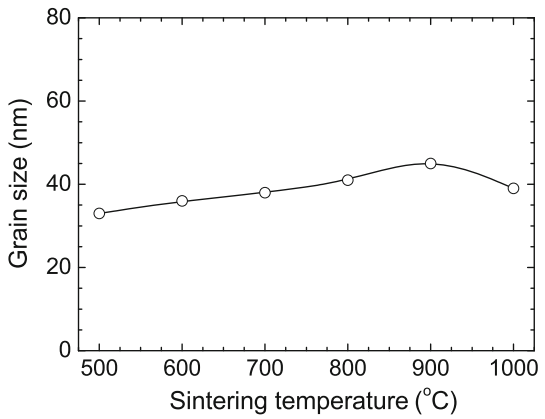

Figure 9 Variation of the grain size of In_2O_3 nanocrystals after SPS treatment at different temperatures.

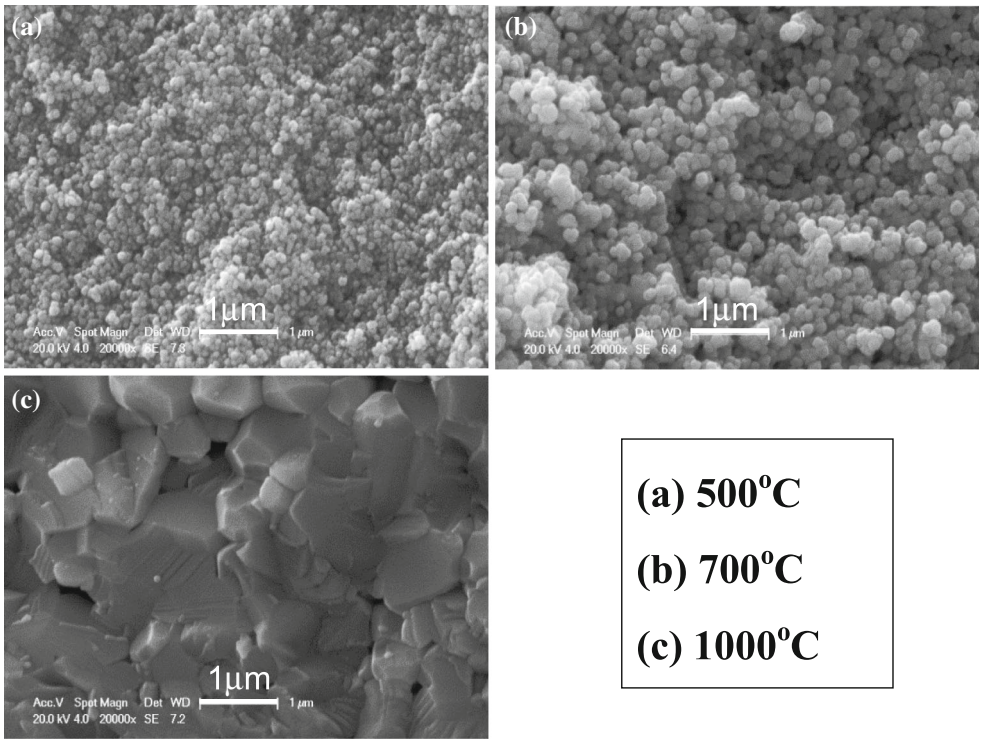

Figure 10 SEM image of In_2O_3 nanocrystals after SPS sintering at **a** 500 °C; **b** 700 °C; **c** 1000 °C.

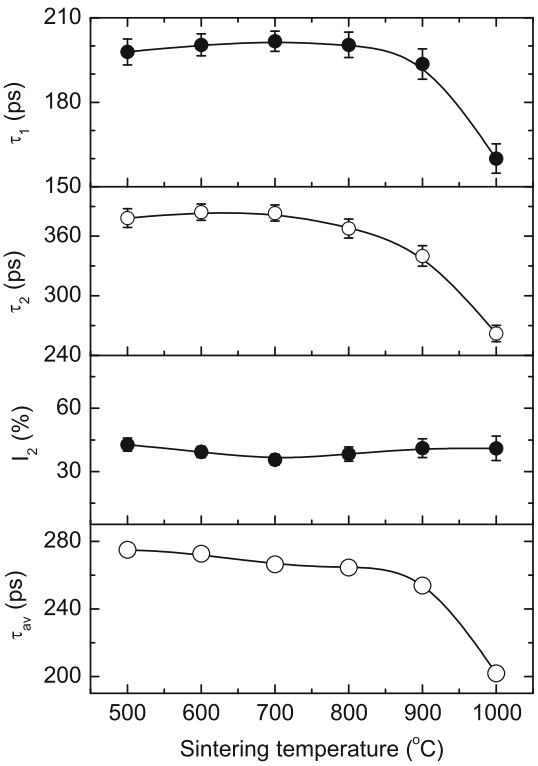

Figure 11 Positron lifetime τ_1, τ_2, intensity I_2 and the average lifetime τ_{av} in In_2O_3 nanocrystals as a function of SPS sintering temperature.

temperature is below 700 °C, then it shows fast decrease with increasing sintering temperature. This is in agreement with the change of τ_1 and τ_2, indicating recovery of monovacancies and vacancy clusters.

The temperature dependence of Seebeck coefficient S, electrical resistivity ρ, total lattice thermal conductivity κ and lattice thermal conductivity κ_L for all the In_2O_3 nanocrystals sintered at different temperatures are shown in Fig. 12. The Seebeck coefficients are all negative in the whole measurement temperature range of 100−600 °C, which indicates that the carriers are electrons. For the samples sintered at 500, 700 and 1000 °C, the electrical resistivity increases monotonically with increasing measurement temperature, which shows the characteristic of metals. It is also clear to see that the electrical resistivity decreases with increasing sintering temperature. This suggests that either more donors are produced, or the mobility of electron increases after high-temperature treatment.

As shown in Fig. 12, the total thermal conductivity κ increases monotonously with increasing sintering temperatures. At measurement temperature of 600 °C, the thermal conductivity increases from 0.6 to 3.5 $Wm^{-1} K^{-1}$ after sintering at 1000 °C. A similar

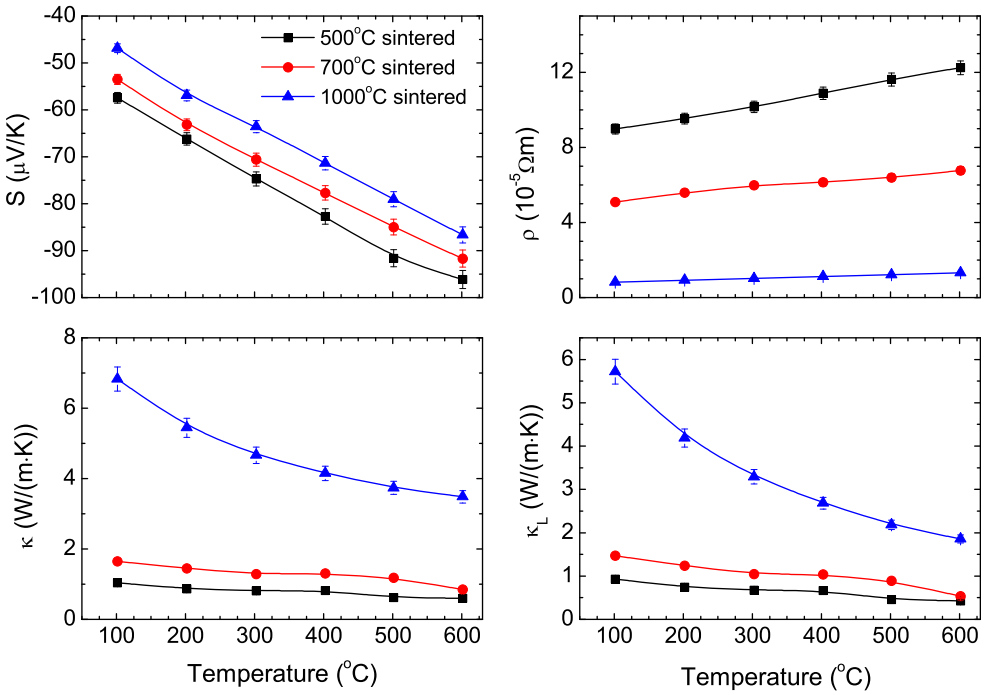

Figure 12 Seebeck coefficient S, electrical resistivity ρ, total thermal conductivity κ and lattice thermal conductivity κ_L of In_2O_3 nanocrystals after SPS sintering at 500, 700 and 1000 °C.

procedure was performed to subtract the contribution of the electronic thermal conductivity κ_E, and the obtained lattice thermal conductivity κ_L of the samples sintered at 500, 700 and 1000 °C is also plotted in Fig. 12. It is found that κ_L increases with the increasing sintering temperature, which shows very similar trend as that of the total thermal conductivity κ. Considering the defect properties revealed by positron annihilation measurements, good correlation between the increase in the lattice thermal conductivity and the recovery of vacancy defects after sintering In_2O_3 nanocrystals at elevated temperatures can be observed once again. However, after sintering at high temperatures, the electrical conductivity shows much larger increase, which compensate for the increase in the thermal conductivity, therefore, the ZT factor plotted in Fig. 13 shows increase at higher sintering temperatures. This is similar to the change of ZT for the samples annealed at different temperatures.

There are several reports of the reduced lattice thermal conductivity in nanocrystalline thermoelectric materials [43–46]. It is generally believed that the grain boundaries are the key factor to reduce lattice thermal conductivity [42]. A large number of experiments have confirmed the decrease in lattice thermal conductivity with decreasing grain size in the nanocrystalline thermoelectric materials [23, 42, 47, 48]. However, in the nanocrystals there are also large amounts of defects

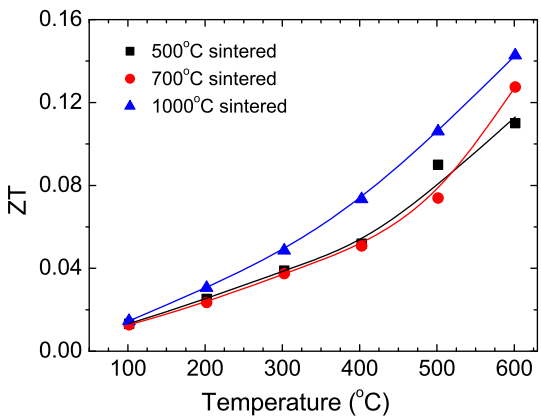

Figure 13 ZT factor of In_2O_3 nanocrystals after SPS sintering at 500, 700 and 1000 °C.

in the grain boundary region. With decreasing grain size, the defect concentration also increases due to increase in the fraction of the grain boundary region. The defects are obviously phonon scattering centers in the nanocrystalline thermoelectric materials [49]. Therefore, it is difficult to clarify whether the effect on lattice thermal conductivity comes mainly from defect or grain boundary scattering. In the present study, we also could not distinguish these two factors for the samples annealed at different temperatures, since the grain size shows considerable increase with increasing annealing temperature. However, for the samples sintered at different temperatures, the grain size has no

obvious change, which indicates that the fraction of grain boundary region is almost the same. Interestingly, the lattice thermal conductivity still shows increase with elevated sintering temperature. This indicates that the change of lattice thermal conductivity is due to other factors instead of grain size effects. Our positron lifetime results clearly indicate that the In monovacancies gradually recover and vacancy clusters also transform into smaller vacancy clusters at higher sintering temperature. Therefore, we can conclude that the increase in lattice thermal conductivity after sintering is mostly due to the recovery of vacancies in the interface region. In other words, the vacancies in the grain boundary region are effective phonon scattering centers in nanocrystalline thermoelectric materials.

Conclusion

In_2O_3 nanopowders were treated with the spark plasma sintering (SPS) at 700 °C followed by annealing at temperatures between 700 and 1300 °C. The average grain size of the annealed samples was obtained by XRD measurements, which increases with increasing annealing temperature. A comparative study is also performed in which the In_2O_3 nanopowders were sintered at temperature between 500−1000 °C. On the contrary, the average grain size of the samples sintered at different temperatures has no obvious change. Positron lifetime measurements reveal monovacancies and vacancy clusters in the nanocrystalline samples, and they gradually recover with increasing thermal treatment temperature. It can be concluded that vacancy-type defects in the grain boundary region play an important role in the lattice thermal conductivity of nanocrystalline In_2O_3.

Acknowledgements

This work was supported by the National Natural Science Foundation of China under Grant Nos. 11475130, 11575131 and 11775163.

References

[1] Nolas GH, Sharp GJ, Goldsmid HJ (2001) Thermoelectrics. Springer, Berlin

[2] Venkatasubramanian R, Siivola E, Colpitts T, O'Quinn B (2001) Thin-film thermoelectric devices with high room-temperature figures of merit. Nature 413:597–602

[3] Bell LE (2008) Cooling, heating, generating power, and recovering waste heat with thermoelectric systems. Science 321:1457–1461

[4] Wang Y, Sui Y, Wang XJ, Su WH, Liu XY (2010) Enhanced high temperature thermoelectric characteristics of transition metals doped $Ca_3Co_4O9+\delta$ by cold high-pressure fabrication. J Appl Phys 107:033708

[5] Mahan GD (1997) Good thermoelectrics. Solid State Phys 51:81–157

[6] Beekman M, Morelli DT, Nolas GS (2015) Better thermoelectrics through glass-like crystals. Nat Mater 14:1182–1185

[7] Callaway J, von Baeyer HC (1960) Effect of point imperfections on lattice thermal conductivity. Phys Rev 120:1149–1154

[8] Klemens PG (1955) The scattering of low-frequency lattice waves by static imperfections. Proc Phys Soc Sect A 68:1113–1128

[9] Abeles B (1963) Lattice thermal conductivity of disordered semiconductor alloys at high temperatures. Phys Rev 131:1906–1911

[10] Pei YZ, Morelli DT (2009) Vacancy phonon scattering in thermoelectric In_2Te_3 CInSb solid solutions. Appl Phys Lett 94:122112

[11] Dasgupta T, Stiewe C, Hassdorf R, Zou AJ, Boettcher L, Mueller E (2011) Effect of vacancies on the thermoelectric properties of $Mg_2Si_{1-x}Sb_x$ ($0 \leq x \leq 0.1$). Phys Rev B 83:235207

[12] Zhu GH, Lan YC, Wang H, Joshi G, Hao Q, Chen G, Ren ZF (2011) Effect of selenium deficiency on the thermoelectric properties of *n*-type In_4Se_{3-x} compounds. Phys Rev B 83:115201

[13] Ji HS, Kim H, Lee C, Rhyee JS, Kim MH, Kaviany M, Shim JH (2013) Effect of selenium deficiency on the thermoelectric properties of n-type In_4Se_{3-x} compounds. Phys Rev B 87:125111

[14] Popuri SR, Scott AJM, Downie RA, Hall MA, Suard E, Decourt R, Pollet M, Bos JWG (2014) Glass-like thermal conductivity in $SrTiO_3$ thermoelectrics induced by A-site vacancies. RSC Adv 4:33720–33723

[15] Bennett NS, Wight NM, Popuri SR, Bosb JWG (2015) Efficient thermoelectric performance in silicon nano-films by vacancy-engineering. Nano Energy 16:350–356

[16] Li W, Lin SQ, Zhang XY, Chen ZW, Xu XF, Pei YZ (2016) Thermoelectric properties of Cu_2SnSe_4 with intrinsic vacancy. Chem Mater 28:6227–6232

[17] Pichanusakorn P, Bandaru P (2010) Nanostructured thermoelectrics. Mater Sci Eng R 67:19–63
[18] Wu Y, Finefrock SW, Yang HR (2012) Nanostructured thermoelectric: opportunities and challenges. Nano Energy 1:651–653
[19] Alam H, Ramakrishna S (2013) A review on the enhancement of figure of merit from bulk to nano-thermoelectric materials. Nano Energy 2:190–212
[20] Fitriani OR, Long BD, Barma MC, Riaz M, Sabri MFM, Said SM, Saidur R (2016) A review on nanostructures of high-temperature thermoelectric materials for waste heat recovery. Renew Sustain Energy Rev 64:635–659
[21] Ren GK, Lan JL, Zeng CC, Liu YC, Zhan B, Butt S, Lin YH, Nan CW (2015) High performance oxides-based thermoelectric materials. JOM 67:211–221
[22] Guilmeau E, Berardan D, Simon C, Maignan A, Raveau B, Ovono D, Delorme F (2009) Tuning the transport and thermoelectric properties of In_2O_3 bulk ceramics through doping at In-site. J Appl Phys 106:053715
[23] Lan JL, Lin YH, Liu Y, Xu SL, Nan CW (2012) High thermoelectric performance of nanostructured In_2O_3-based ceramics. J Am Ceram Soc 95:2465–2469
[24] Dupasquier A, Mills AP Jr (1995) Positron spectroscopy of solids. IOS Press, Amsterdam
[25] Krause-Rehberg R, Leipner HS (1999) Positron annihilation in semiconductors, defect studies, springer series in solid-state sciences, vol 127. Springer, Berlin
[26] Nambissan PMG, Upadhyay C, Verma HC (2003) Positron lifetime spectroscopic studies of nanocrystalline $ZnFe_2O_4$. J Appl Phys 93:6320–6326
[27] Chakrabarti S, Chaudhuri S, Nambissan PMG (2005) Positron annihilation lifetime changes across the structural phase transition in nanocrystalline Fe_2O_3. Phys Rev B 71:064105
[28] Biswas S, Kar S, Chaudhuri S, Nambissan PMG (2006) Positron annihilation studies of defects and interfaces in ZnS nanostructures of different crystalline and morphological features. J Chem Phys 125:164719
[29] Dutta S, Chattopadhyay S, Jana D, Banerjee A, Manik S, Pradhan SK, Sutradhar M, Sarkar A (2006) Annealing effect on nano-ZnO powder studied from positron lifetime and optical absorption spectroscopy. J Appl Phys 100:114328
[30] Mishra AK, Chaudhuri SK, Mukherjee S, Priyam A, Saha A, Das D (2007) Characterization of defects in ZnO nanocrystals: photoluminescence and positron annihilation spectroscopic studies. J Appl Phys 102:103514
[31] Ghoshal T, Biswas S, Kar S, Chaudhuri S, Nambissan PMG (2008) Positron annihilation spectroscopic studies of solvothermally synthesized ZnO nanobipyramids and nanoparticles. J Chem Phys 128:074702
[32] Wang D, Chen ZQ, Wang DD, Qi N, Gong J, Cao CY, Tang Z (2010) Positron annihilation study of the interfacial defects in ZnO nanocrystals: correlation with ferromagnetism. J Appl Phys 107:023524
[33] Chaudhuri SK, Ghosh M, Das D, Raychaudhuri AK (2010) Probing defects in chemically synthesized ZnO nanostrucures by positron annihilation and photoluminescence spectroscopy. J Appl Phys 108:064319
[34] Cullity BD (1978) Elements of X-ray diffraction, vol 9. Addison-Wesley, Philippines, p 284
[35] Kirkegaard P, Pederson NJ, Eldrup M (1989) Risϕ Report M2740; Risϕ National Laboratory: DK-4000 Roskilde, Denmark
[36] Sanyal D, Banerjee D, De U (1998) Probing $(Bi_{0.92}Pb_{0.17})_2Sr_{1.91}Ca_{2.03}Cu_{3.06}O_{10+\delta}$ superconductors from 30 to 300 K by positron-lifetime measurements. Phys Rev B 58:15226–15230
[37] de la Cruz RM, Pareja R, Gonzalez R, Boatner LA, Chen Y (1992) Effect of thermochemical reduction on the electrical, optical-absorption, and positron-annihilation characteristics of ZnO crystals. Phys Rev B 45:6581–6586
[38] Korhonen E, Tuomisto F, Bierwagen O, Speck JS, Galazka Z (2014) Compensating vacancy defects in Sn- and Mg-doped In_2O_3. Phys Rev B 90:245307
[39] Puska MJ, Nieminen RM (1994) Theory of positrons in solids and on solid surfaces. Rev Mod Phys 66:841–897
[40] Puska MJ, Nieminen RM (1983) Defect spectroscopy with positrons: a general calculational method. J Phys F Met Phys 13:333–346
[41] Tomita T, Yamashita K, Hayafuji Y, Adachi H (2005) The origin of n-type conductivity in undoped In_2O_3. Appl Phys Lett 87:051911
[42] Takashiri M, Miyazaki K, Tanaka S, Kurosaki J, Nagai D, Tsukamoto H (2008) Effect of grain size on thermoelectric properties of n-type nanocrystalline bismuth-telluride based thin films. J Appl Phys 104:084302
[43] Takashiri M, Borca-Tasciuc T, Jacquot A, Miyazaki K, Chen G (2006) Structure and thermoelectric properties of boron doped nanocrystalline $Si_{0.8}Ge_{0.2}$ thin film. J Appl Phys 100:54315
[44] Wang XW, Lee H, Lan YC, Zhu GH, Joshi G, Wang DZ, Yang J, Muto AJ, Tang MY, Klatsky J, Song S, Dresselhaus MS, Chen G, Ren ZF (2008) Enhanced thermoelectric figure of merit in nanostructured n-type silicon germanium bulk alloy. Appl Phys Lett 93:193121
[45] Poudel B, Hao Q, Ma Y, Lan YC, Minnich A, Yu B, Yan X, Wang DZ, Muto A, Vashaee D, Chen XY, Liu JM, Dresselhaus MS, Chen G, Ren ZF (2008) High-thermoelectric performance of nanostructured bismuth antimony telluride bulk alloys. Science 320:634–638

[46] Bux SK, Blair RG, Gogna PK, Lee H, Chen G, Dresselhaus MS, Kaner RB, Fleurial JP (2009) Nanostructured bulk silicon as an effectivethermoelectric material, fleurial. Adv Funct Mater 19:2445–2452

[47] Chiritescu C, Mortensen C, Cahill DG, Johnson D, Zschack P (2009) Lower limit to the lattice thermal conductivity of nanostructured Bi_2Te_3-based materials. J Appl Phys 106:073503

[48] Foley BM, Brown-Shaklee HJ, Duda JC, Cheaito R, Gibbons BJ, Medlin D, Ihlefeld JF, Hopkins PE (2012) Thermal conductivity of nano-grained $SrTiO_3$ thin films. Appl Phys Lett 101:231908

[49] Lan YC, Minnich AJ, Chen G, Ren ZF (2010) Enhancement of thermoelectric figure-of-merit by a bulk nanostructuring approach. Adv Funct Mater 20:357–376